Discover Chemistry

RESEARCH Open Access

Biochar derived from bean husk for the removal of lead and hexavalent chromium from aqueous solutions

Hussein K. Okoro[1,2], Ebuka Chizitere Emenike[1*], Kingsley O. Iwuozor[1], Joshua Emeghai[3,4], Caliphs Zvinowada[5], Catherine J. Ngila[5] and Adewale George Adeniyi[6]

*Correspondence:
Ebuka Chizitere Emenike
emenikechizitere@gmail.com
[1]Department of Industrial Chemistry, University of Ilorin, P. M. B. 1515, Ilorin, Nigeria
[2]Department of Chemistry and Industrial Chemistry, Kwara State University, P.M. B 1530, Malete, Nigeria
[3]Department of Structural Engineering, University of Benin, Benin, Edo State, Nigeria
[4]Department of Construction Management, Louisiana State University, Baton Rouge, USA
[5]Department of Chemical Sciences, Faculty of Science, University of Johannesburg, P.O. Box 17011, Doornfontein, Johannesburg 2028, Republic of South Africa
[6]Department of Chemical Engineering, Faculty of Engineering and Technology, University of Ilorin, P. M. B. 1515, Ilorin, Nigeria

Abstract

Heavy metals are among the most prevalent and difficult environmental pollutants to manage. This study explored the conversion of bean husks into biochar and evaluated its effectiveness as an inexpensive adsorbent to eliminate Pb(II) and Cr(VI) from water. Several analytical methods were utilized to ascertain the properties of the bean husk-based biochar (BHB), while sorption performance was evaluated under different conditions, including contact time, solution pH, biochar dosage, starting metal concentrations, and temperature. The findings revealed that BHB had a surface area of 24.28 m^2/g and a pore volume of 0.5105 cm^3/g, and achieved removal efficiencies of 94.7% for Pb(II) and 91.5% for Cr(VI) under optimal conditions. Several kinetic and equilibrium isotherm models were also employed to interpret the uptake behavior. The highest uptake capacities recorded for Pb(II) and Cr(VI) were 18.38 mg/g and 22.78 mg/g, respectively, with the isotherm closely matching the Freundlich model. Kinetic modeling revealed that Pb(II) uptake conformed more closely to the pseudo-second-order model, while Cr(VI) aligned with the pseudo-first-order model. Regeneration tests showed that the biochar retained more than 60% of its initial performance after three reuse cycles for both metal ions, indicating good reusability for a non-activated, agriculturally derived adsorbent. The sorption mechanism involved a combination of ion exchange, surface complexation, electrostatic interactions, and physical attraction via van der Waals forces.

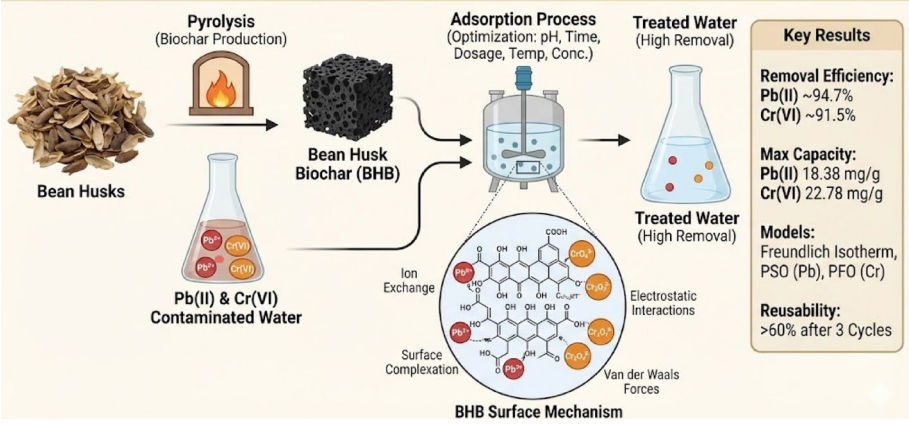
Keywords Kinetics, Isotherm modeling, Heavy metals, Adsorption, Mechanism

1 Introduction

The aquatic ecosystem is constantly being exposed to a vast variety of pollutants, mostly as a result of rising industrialization, rapid population growth, excessive use of natural resources, technological advancements, and agricultural practices. Among these pollutants, heavy metals are especially dangerous because of their longevity, non-biodegradability, toxicity, and capacity to build up in biological tissues, leading to magnification within the food chain [1–3]. Among them, lead and chromium are among the most commonly detected in water. Lead (Pb) is a metal with a low melting point that has

© The Author(s) 2026. **Open Access** This article is licensed under a Creative Commons Attribution-NonCommercial-NoDerivatives 4.0 International License, which permits any non-commercial use, sharing, distribution and reproduction in any medium or format, as long as you give appropriate credit to the original author(s) and the source, provide a link to the Creative Commons licence, and indicate if you modified the licensed material. You do not have permission under this licence to share adapted material derived from this article or parts of it. The images or other third party material in this article are included in the article's Creative Commons licence, unless indicated otherwise in a credit line to the material. If material is not included in the article's Creative Commons licence and your intended use is not permitted by statutory regulation or exceeds the permitted use, you will need to obtain permission directly from the copyright holder. To view a copy of this licence, visit http://creativecommons.org/licenses/by-nc-nd/4.0/.

Graphical Abstract



a bluish-grey appearance [4]. It enters the ecosystem from a variety of anthropogenic pathways, including industrial operations, smelting, tainted food, lead-based paints, tobacco smoke, and the use of leaded fuels. Pb is a non-essential element that impairs various physiological functions, including the reproductive, neurological, hematologic, and cardiovascular systems when it is present in the human body, even at low concentrations [4, 5]. Pb ranks first on the list of dangerous compounds compiled by the U.S. Agency for Toxic substances and Disease Registry (ATSDR) [6]. Similarly, chromium (Cr) is a metal that has been used extensively in across different sectors, including brass, pigments, catalysis, metal finishing, wood-based materials maintenance, leather processing, pulp manufacturing, steel processing, and textile printing, among others [7–9]. Hexavalent chromium [Cr(VI)] and trivalent chromium [Cr(III)] are the two primary forms of Cr found in the environment. With regard to this, Cr(VI) is recognized for its cancer-causing and mutation-causing properties. It is also a potent oxidizer that can irritate plant and animal tissues, even at extremely trace levels, and is a hundredfold more perilous than Cr(III) [7, 10, 11]. To safeguard public health, maximum contamination levels of 0.015 mg/L and 0.1 mg/L, respectively, were set for Pb(II) and Cr(VI) by the US Environmental Protection Agency (EPA) [12].

Adsorption stood out among the various techniques used for eliminating Pb(II) and Cr(VI) ions from water and has been gaining popularity due to its capacity to work at low concentrations with shorter operating times and considerably less expense than other means of treatment [13, 14]. In order to create technically and financially viable water treatment methods, adsorption process engineering typically entails a number of variables that need to be examined and optimized [15]. Choosing an effective adsorbent material that has appropriate sorption sites for the adsorbate is one of these criteria. Optimal adsorbents should have great physical or chemical stability and a large specific surface area. In addition, the material ought to have a substantial adsorption capacity and be affordable, safe to use, sustainable, selective, and eco-friendly [16, 17]. While activated carbon is a well-established adsorbent, its high cost has prompted researchers to explore more affordable and sustainable alternatives. One promising option is biochar, which shares several characteristics with activated carbon and is gaining recognition as a cost-effective substitute.

Biochar refers to a solid, carbon-dense material produced through thermochemically converting biomass under conditions of no or minimal oxygen supply. Its adsorption capacity is closely related to its physicochemical properties, including total surface area, pore structure, existence of surface functional groups, and its capacity for cation exchange [18, 19]. Heavy metal ions can readily penetrate biochar due to its interconnecting pores and nanoscale porous nature. Biochar's functional groups, which are abundant in nitrogen, phosphorus, and sulfur, among other elements, can interact with the metal ions through complexation, limiting the metals' mobility [20, 21]. Biochar can be created from a variety of feedstocks, such as digestate, energy crops, dung, activated sludge, forest waste, algal biomass, and agricultural residues [22, 23]. Among these, agricultural residues, such as peels, stems, leaves, pods, and husks, are among the most commonly used sources.

Bean husks are an agricultural residue generated during the processing of beans (*Phaseolus vulgaris*), a highly nutritious food. With global annual production of common beans reaching approximately 27 million tonnes, a substantial amount of husk waste is produced during harvesting and grain separation [24]. Although bean husks can be used as an animal feed supplement, they hold minimal economic value and are often discarded in landfills, contributing to environmental pollution [25, 26]. Converting bean husks into biochar presents a sustainable approach to recycling this agricultural waste.

Although numerous studies have reported the removal of Pb(II) and Cr(VI) using biochars derived from diverse agricultural residues, much of this work relies on chemically activated or surface-modified materials that require additional reagents, higher energy input, and greater production costs [27–29]. These factors limit their applicability in settings where low-cost and locally available adsorbents are essential. Bean husk, despite being generated in large quantities and possessing a favourable lignocellulosic composition [30], remains largely underexplored as a precursor for biochar production. Furthermore, no comprehensive study has evaluated its capacity to remove both Pb(II) and Cr(VI), nor examined the underlying adsorption mechanisms through kinetic, isotherm, thermodynamic, and regeneration analyses. This gap highlights the need to assess bean husk biochar as a simple, sustainable, and economically practical adsorbent. The present study therefore aims to synthesise biochar from bean husk, characterise its physicochemical properties, evaluate its performance toward Pb(II) and Cr(VI) removal, and examine its reusability and adsorption mechanisms, with a view toward future development of affordable wastewater treatment materials.

2 Materials and methods

2.1 Materials and chemicals

Bean husks (BH) utilized in this research were sourced from a local marketplace in Ogbomosho, Nigeria. The study utilized lead(II) nitrate ($Pb(NO_3)_2$) and potassium dichromate ($K_2Cr_2O_7$) as the primary reagents. Every chemical utilized was of analytical quality and did not require any further purification.

2.2 Biochar production

The bean husks were initially rinsed with tap water and then with distilled water to eliminate surface contaminants and other unwanted residues. After cleaning, the materials were sun-dried until a stable weight was achieved. Biochar was produced from

the feedstock using top-lit updraft reactor as previously outlined by Emenike et al. [31]. The reactor is shown in Fig. 1. The setup includes an internal chamber for loading the biomass and a combustion zone that contains the heating fuel, which thermally decomposes the biomass in the inner chamber through indirect (retort) heating, and the exhaust fume at the center of the lid, which allows for the elutriation of the combustion gases. Air is introduced through perforations at the reactor's base and moves upward to sustain the combustion zone positioned above, resulting in an updraft mode of operation. 100 g of the dried bean husks were fed into the inner carbonization chamber while the fuel (stems of *Delonix regia*) was contained in the combustion chamber, and the process operated for 110 min. The reactor temperature was monitored with a CASON CA380 infrared thermometer, resulting in a peak temperature of 320 ℃. At expiration, the resultant biochar was collected and preserved in a tightly sealed container for subsequent analysis. This biochar derived from bean husk was designated as BHB.

2.3 Biochar characterization

A muffle furnace was employed to perform the proximate assessment of biochar utilizing the ASTM D-5142 method, as described by Jian et al. [32]. Moisture content was assessed by drying the samples in an uncovered crucible at 105 °C until a stable weight was reached. Volatile matter was evaluated based on the weight reduction of the biochar after heating it in a sealed crucible at 900 °C for a duration of 7 min. Ash content was determined as the remaining mass after heating the sample in an open crucible to 600 °C and maintaining that temperature until the weight stabilized. Finally, the fixed carbon content was ascertained indirectly by deducting the measured values of moisture, volatile matter, and ash from 100%. Fourier transform infrared spectroscopy (FTIR) analysis was conducted utilizing a Shimadzu FTIR-8400 S spectrometer to elucidate the surface chemistry and functional groups present in BHB. The dried biochar samples were finely powdered, mixed with spectroscopic-grade KBr, and pressed into transparent pellets using a hydraulic press before spectral acquisition. At an 8 cm^{-1} resolution, the spectra were captured in the 400–4000 cm^{-1} wavenumber range. Additionally, a TESCAN VEGA3 scanning electron microscope (SEM) was used to analyze the surface morphology of BHB. Prior to SEM imaging, the biochar samples were gently ground, mounted on carbon-adhesive stubs, and sputter-coated with a thin layer of gold to enhance surface

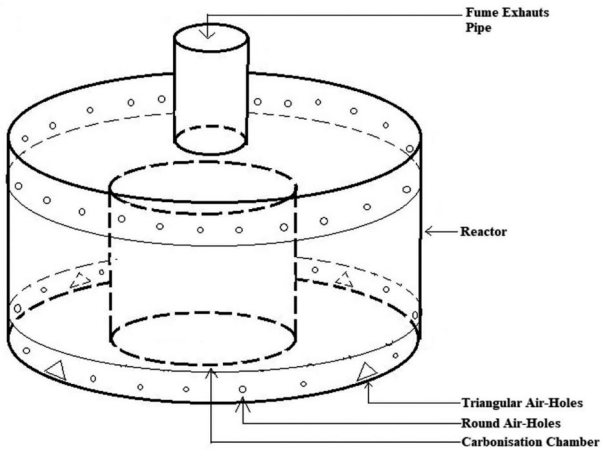


Fig. 1 An overview of the reactor used for biochar production

conductivity and prevent charging during analysis. When used in conjunction with an energy dispersive X-ray spectroscopy (EDS) system, this device made it easier to qualitatively analyze the sample's elemental makeup. The identification of elemental oxides and inorganic constituents was carried out with X-ray fluorescence spectrometer (Bruker XRF Instruments, Australia). The Brunauer-Emmett-Teller (BET) surface area and pore structure analysis were performed using a Quantachrome NovaWin (version 11.03) analyzer. Prior to measurement, samples were degassed at 200 °C for 4 h under vacuum to remove physisorbed moisture and volatile residues. Nitrogen gas (N_2) was used as the adsorbate at a measurement temperature of 77 K. Adsorption–desorption isotherms were generated to evaluate the specific surface area using the BET model, while pore volume and pore diameter were derived from the Barrett-Joyner-Halenda (BJH) method.

2.4 pH_{pzc} determination

The drift method was employed to determine the biochar's point of zero charge (pH_{pzc}) [33]. 10 Erlenmeyer flasks were set up, each comprising 20 mL of a 100 mg/L metal ion solution. Utilizing 0.1 M HCl and NaOH, the original pH of these solutions was brought within the range of 2–12. Afterward, the corresponding flasks were filled with 0.5 g of the biochar and shaken for three hours at 200 rpm in an orbital shaker. The final pH values were measured at equilibrium. The overall experimental workflow, from bean husk processing to biochar synthesis, characterization, adsorption testing, and regeneration, is presented in Fig. 2.

2.5 Adsorption experiment

To assess the capability of BHB to uptake Pb(II) and Cr(VI) from water, batch adsorption experiments were conducted. Reagent-grade $Pb(NO_3)_2$ and $K_2Cr_2O_7$ were dissolved in distilled water to create initial stock solutions of 1000 mg/L. These stock solutions were then diluted to the appropriate concentrations in accordance with the experimental requirements. For each test, 0.5 g of biochar was introduced into 20 mL of a 100 mg/L metal solution. Pb(II) and Cr(VI) were treated in separate Erlenmeyer flasks. A solution of 0.5 M HCl and 0.5 M NaOH was used to alter the original pH. The prepared

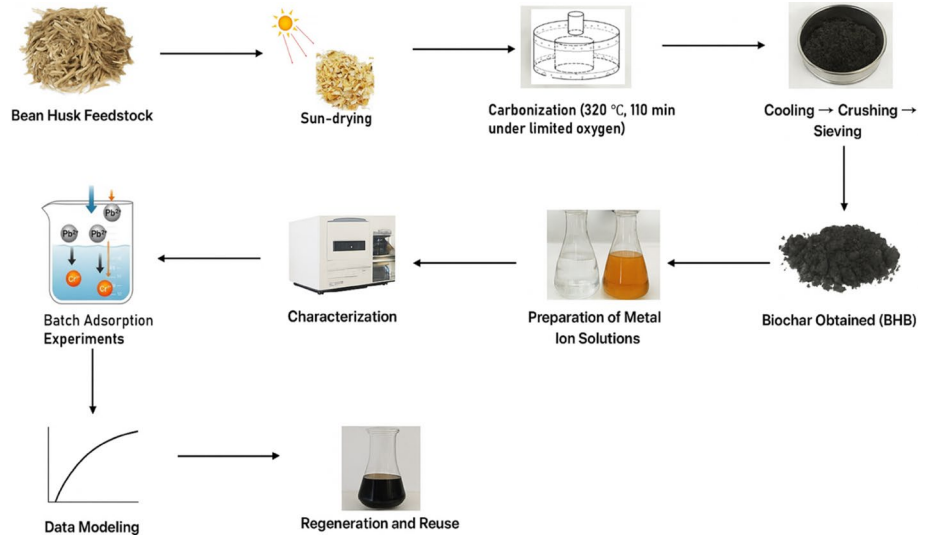


Fig. 2 A schematic illustration of the batch adsorption setup employed in this study

flasks were then placed on an orbital shaker and shaken at a constant speed of 200 rpm for 50 min at ambient temperature (25 °C). After shaking, the mixtures were filtered, and an atomic absorption spectrophotometer (BUCK Scientific ACCUSYS 211 model) was utilized to evaluate the filtrates to ascertain the residual quantities of Pb(II) and Cr(VI) ions. Before sample measurement, the instrument was calibrated using external standards freshly prepared from the 1000 mg/L stock solutions. Calibration curves were constructed over appropriate working ranges (0–10 mg/L for Pb and 0–5 mg/L for Cr), each containing at least five points with determination coefficients (R^2) greater than 0.999. Analytical blanks were run to correct for baseline drift, and calibration was repeated after every ten samples to ensure signal stability. Pb(II) was measured at its primary resonance line of 283.3 nm, while Cr(VI) was assessed at 357.9 nm, both under an air–acetylene flame.

The study examined various influencing factors, including: (1) the effect of pH, where 0.5 g of biochar was introduced into 20 mL of 100 mg/L Pb(II) and Cr(VI) solutions at 25 °C, with pH adjusted to 2, 3, 5, 8, and 9 using 0.5 M HCl and 0.5 M NaOH; (2) the impact of biochar dosage, with 0.1, 0.3, 0.5, 0.7, and 0.9 g added at 25 °C; (3) adsorption isotherm studies, where 20 mL solutions of each metal ion at varying concentrations (20–100 mg/L) were prepared at 25 °C; (4) sorption kinetics, using 0.5 g of BHB at 25 °C, with contact times of 10, 20, 30, 40, and 50 min; and (5) the effect of temperature, where 0.5 g of BHB was used and temperatures were adjusted to 25, 30, 40, 50, and 60 °C in a water bath. All samples were subjected to agitation for 50 min. The amount of Pb(II) and Cr(VI) ions removed, along with the corresponding percentage of removal, was computed by comparing the concentrations before and after treatment, as described by Eqs. 1 and 2.

$$q_e = (C_O - C_e)\frac{V}{M} \tag{1}$$

$$q_{\%} = \frac{(C_O - C_e)}{C_O} \times 100 \tag{2}$$

In these expressions, $C_o$and C_e denote the original and equilibrium concentrations of the metal ions in mg/L. V refers to the volume of the solution in liters, while *m* represents the amount of BHB used in mg. When measurements were taken at a particular time t, C_e becomes C_t.

2.6 Adsorption isotherms

To investigate the sorption equilibrium, the experimental data were applied to the linearized equations of three isotherm models: Langmuir, Freundlich, and Temkin. The fitting parameters from these models were employed to characterize the sorption process and learn more about the sorption mechanism. The corresponding linear equations for each model are given as Eqs. 3, 4, and 5, respectively, referencing the Langmuir, Freundlich, and Temkin models [34, 35].

Langmuir model:

$$\frac{C_e}{q_e} = \frac{1}{K_L q_m} + \frac{1}{q_m} C_e \tag{3}$$

Freundlich model:

$$In\,(q_e) = InK_F + \frac{1}{n}InC_e \tag{4}$$

Temkin model:

$$q_e = \frac{RT}{b}InK_T + \frac{RT}{b}InC_e \tag{5}$$

where q_e denotes the amount of adsorbate retained per gram of adsorbent at equilibrium (mg/g), C_e stands for the equilibrium amount of metal ions in the solution (mg/L), K_L is the Langmuir constant related to adsorption affinity (L/mg), and q_m is the calculated monolayer adsorption capacity (mg/g). K_f represents the Freundlich constant, $1/n$ represents the heterogeneity factor. The universal gas constant is represented by R (8.314 J/mol.K), T denotes temperature in Kelvin, K_T is the Temkin equilibrium binding constant, and b is associated with the heat of adsorption (J/mol).

2.7 Adsorption kinetics

Kinetic analysis was assessed by applying the data to the linearized versions of commonly used kinetics, such as the pseudo-first-order, pseudo-second-order, intraparticle diffusion, and Elovich, with their respective expressions shown in Eqs. 6, 7, 8, and 9 [36].

Pseudo-first-order (PFO):

$$Log\,(q_e - q_t) = Logq_e - \frac{K_1}{2.303}t \tag{6}$$

Pseudo-second-order (PSO):

$$\frac{t}{q_t} = \frac{1}{K_2 q_e^2} + \frac{1}{q_e}t \tag{7}$$

Intraparticle diffusion (IPD):

$$q_t = K_{dif}t^{1/2} + C \tag{8}$$

Elovich model:

$$q_t = \frac{1}{\beta}In\,(\alpha\,\beta\,) + \frac{1}{\beta}In\,(t) \tag{9}$$

In these equations, $K_1(\text{min}^{-1})$ represents the rate constant for PFO model, while q_e and q_t (mg/g) denote the quantity of the compound adsorbed by the biochar at equilibrium and at a specific time t (minutes), respectively. K_2 corresponds to the rate constant for PSO model ($\text{mg}^{-1}\text{min}^{-1}$). C is a constant that provides insight into the boundary layer's thickness surrounding the adsorbent particles and K_{dif} ($\text{mg/gmin}^{1/2}$) is the IPD rate constant. α is the initial adsorption rate (mg/g.min), β is the desorption constant (g/mg).

2.8 Thermodynamic study

The characteristics of Pb(II) and Cr(VI) sorption on the biochar adsorbent were calculated using the thermodynamic expression shown in Eq. 10, with K_c representing thermodynamic equilibrium constant [37].

$$K_c = \frac{C_o - C_e}{C_e} \tag{10}$$

Gibbs free energy change (ΔG) is connected to K_c through Eqs. 11 and 12, with Eq. 12 known as the Van't Hoff Eq.

$$\Delta G = -RTInK_c \tag{11}$$

$$InK_c = -\frac{\Delta G}{RT} = \frac{\Delta S}{R} - \frac{\Delta H}{RT} \tag{12}$$

where C_o and C_e represent the starting and final concentrations of the metal ions in solution, respectively. ΔH indicates the change in enthalpy, while ΔS denotes the change in entropy. R represents the universal gas constant (8.314 J/mol.K), and T is the absolute temperature measured in Kelvin. The values of ΔS and ΔH are derived from the intercept and slope, respectively, of the linear plot of InK_c against $\frac{1}{T}$.

2.9 Desorption and reusability study

To evaluate the potential for repeated use of the biochar adsorbent, regeneration and desorption tests were conducted employing HNO_3 as the desorbing agent. The spent biochar was immersed in 20 ml of a 0.1 HNO_3 solution, shaken for 2 h in an orbital shaker at 200 rpm and then separated by filtration. The desorption efficiency was determined by analyzing the metal ion concentrations in the eluents. The regenerated biochar was then tested for its adsorption capacity over three adsorption-desorption cycles. Before each adsorption cycle, the biochar was oven-dried at 130 °C for 2 h and subsequently utilized again in the adsorption and desorption of Pb(II) and Cr(VI). Equation 13 was used to determine the desorption efficiency (D).

$$D\,(\%) = \frac{M_a}{M_d} \times 100 \tag{13}$$

Here, M_a is the quantity of metal ion retained during a given cycle, while M_d denotes the quantity adsorbed initially.

3 Results and discussions

3.1 Characterization of bean husk biochar (BHB)

3.1.1 Biochar yield, proximate analysis, and specific surface area

As shown in Table 1, the biochar production process lasted for 110 min, achieving a yield of 38.4% at the maximum temperature of 320 ℃. This value is consistent with most previous biomass-based biochar made with similar methods, including corn husk (37.8%)

Table 1 Proximate and BET analyses of BH and BHB

Parameter	BH	BHB
Biochar yield (%)	–	38.4
Moisture (%)	7.42	6.82
Volatile matter (%)	57.86	27.20
Fixed carbon (%)	11.50	44.96
Ash	23.23	21.03
BET surface area (m^2/g)	3.36	24.28
Pore volume (cm^3/g)	0.0037	0.5105
Pore size (nm)	32.73	13.12

[38], sugarcane bagasse (16.67%) [39], and coconut fibres (30.2%) [40], among others. Hence, it can be surmised that bean husk is a viable feedstock for biochar production. It has been suggested that such low temperature observed in this study is ideal for high biochar yield [41].

Table 1 also provides the proximate analysis results for both the rice husk feedstock and the resulting biochar. The raw feedstock has a moisture content of 7.42%, which slightly decreased to 6.82% after carbonization. The volatile matter, on the other hand, decreased significantly from 57.86% in raw bean husk to 27.20% in the biochar. The carbonization temperature and volatile matter content are typically correlated; the greater the temperature, the more volatile matter is extracted from the feedstock. A feedstock material with good carbon adsorbent potential is indicated by elevated volatile matter and modest ash concentration [32]. The ash component of both the BH and BHB is relatively high, which is an indication of higher inorganic compounds in the samples [42]. High fixed carbon of 44.96% can be observed in the biochar, which suggests a successful carbonization. The process of converting raw biomass into biochar fixes or concentrates its carbon content [19].

The BET technique was employed to assess the surface area and porosity of both the raw bean husk and the produced biochar, with the findings summarized in Table 1. The specific surface areas for BH and BHB were found to be 3.36 m^2/g and 24.28 m^2/g, respectively, while their pore volumes were recorded at 0.0037 cm^3/g and 0.5105 cm^3/g. The carbonization process substantially enhanced the porosity of the material, leading to an over sevenfold increase in surface area and nearly a 140-fold rise in pore volume compared to the raw feedstock. A larger surface area suggests a greater number of available binding sites for capturing contaminants. This expansion in surface area is usually accompanied by an enhancement in pore volume and a drop in pore diameter [43]. This explains the significant decrease in the pore size of biochar (13.12 nm) compared to that of the raw biomass (32.73 nm).

3.1.2 FTIR analysis

Figure 3a displays the spectrum from the FTIR study that was done to identify the functional groups in BHB. O-H stretching vibrations are responsible for the high intensity peak at 3435 cm^{-1}, which suggests the existence of hydroxyl groups. The minor peaks at 3027 and 2970 cm^{-1} represents symmetrical C-H stretching vibrational peaks of -CH_2 groups, whereas C≡C stretching of alkynes is responsible for the band at 2066 cm^{-1} [44]. Stretching vibrations of carbonyl groups (C = O) associated with ketones, aldehydes, esters, and carboxylic anhydrides are represented by the peak at 1738 cm^{-1}, whereas aromatic C = C stretch vibrations of carboxylic acids are assigned to the peak at 1601 cm^{-1} [26, 45]. Several other groups can be observed in the fingerprint region of the spectrum. The absorption bands at 1384 cm^{-1} and 1216 cm^{-1} are likely associated with aromatic C-H stretch and C-O groups of secondary alcohols, respectively, which are commonly found in lignocellulosic-based materials [26, 46]. Several out of plane deformation peaks, such as 873 cm^{-1}, 644 cm^{-1}, and 540 cm^{-1}, corresponding to aromatic C-H vibrations were also observed.

The FTIR spectrum of the adsorbent after adsorption (Fig. 3b) revealed a significant shift in the peaks. The broad O-H band shifts from 3435 to 3305 cm^{-1} after adsorption, indicating participation of hydroxyl groups through hydrogen bonding, deprotonation

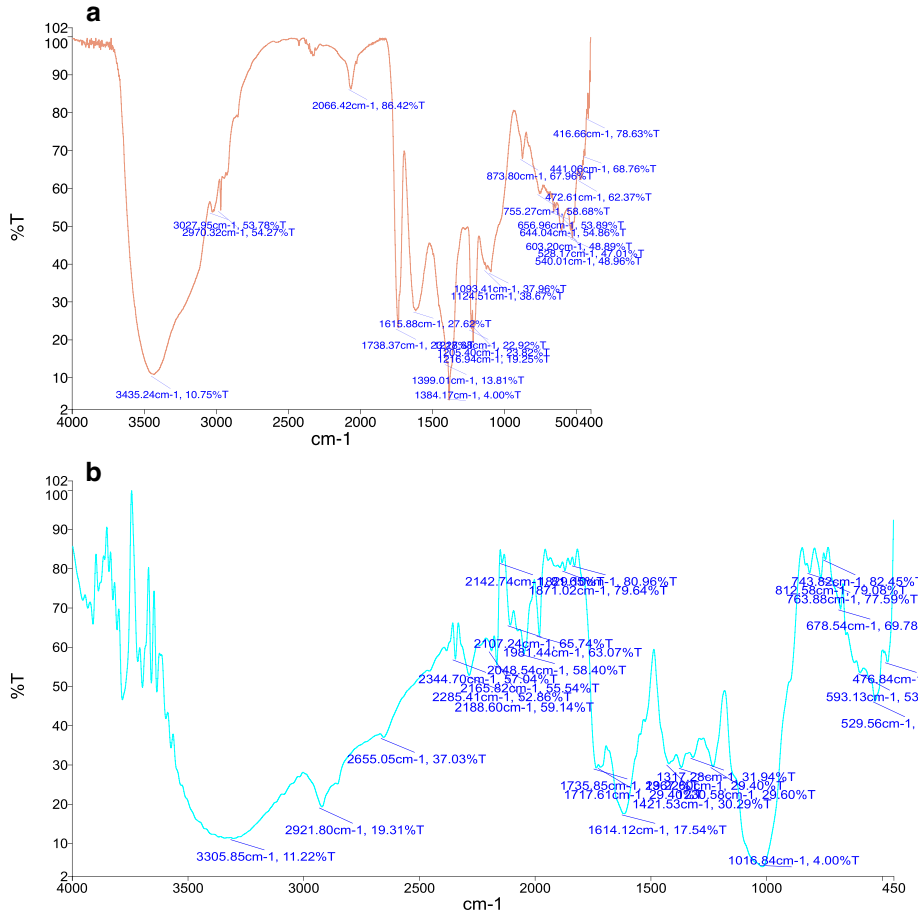
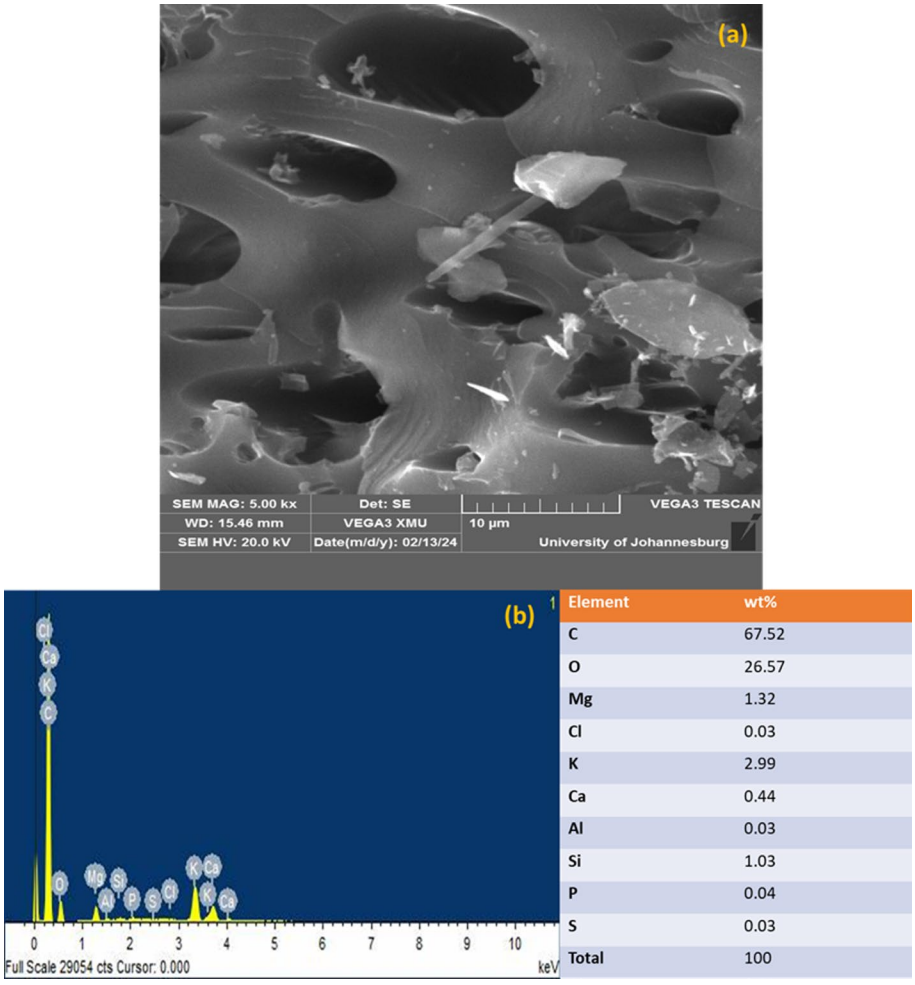


Fig. 3 FTIR spectra of BHB before **a** and after **b** adsorption

or direct coordination. The carbonyl band at 1738 cm^{-1} and the aromatic/carboxylate region near 1601 cm^{-1} show small but measurable shifts (to 1735 and 1614 cm^{-1}, respectively), consistent with changes in electron density following complexation. There is a significant reorganisation in the fingerprint region (1216 shifts to 1317 cm^{-1} and appearance of a band at 1016 cm^{-1}), which points to involvement of C–O and phenolic groups. New low-frequency bands at 593 and 529 cm^{-1} appear after adsorption; these are characteristic of metal-oxygen vibrations and provide direct spectroscopic evidence for formation of surface-bound Pb-O and Cr-O species.

3.1.3 SEM and EDX analyses

The SEM photograph of BHB is shown in Fig. 4a. The biochar showed a smooth surface morphology with a well-developed porous network. The pores are large and irregular, indicating the biochar's ability as an effective adsorbent. There is also the presence of some whitish specks on the surface, which may be related to the presence of some residual elements. EDX analysis was used to validate the existence of these elements, and the results, along with the EDX spectrum, are displayed in Fig. 4b. As can be seen, carbon is the predominant element, constituting about 67.59% of the elements. This indicates successful conversion of bean husk into biochar, a carbon-rich material. Besides, raw bean husk has been reported to contain as high 84.21% carbon [26]. Oxygen is the next common element in the biochar, and can be present in the form of hydroxyl (-OH) or



Element	wt%
C	67.52
O	26.57
Mg	1.32
Cl	0.03
K	2.99
Ca	0.44
Al	0.03
Si	1.03
P	0.04
S	0.03
Total	100

Fig. 4 Morphology and elemental analysis of BHB showing **a** SEM image and **b** EDX spectrum

carbonyl (C = O) groups. Such oxygen-based groups are abundant in lignocellulosic biomass such as BH. Several other elements like magnesium, chlorine, potassium, among others, are detected in trace amounts. The presence of these elements can be responsible to the high content of ash in BHB, as observed in the proximate analysis.

3.1.4 XRF analysis

The XRF analysis of the biochar shows the presence of various oxides, as shown in Table S1. Among them, K_2O, CaO, SiO_2, and MgO are the major components. The high abundance of potassium oxide (K_2O) indicates a high content of potassium, which is common in plant-derived biochars. Calcium oxide (CaO), on the other hand, contributes to the biochar's alkalinity and enhancing its adsorption capacity for heavy metals [47], while silicon dioxide (SiO_2) indicates the presence of silica. Silicon is deemed as a significant ash constituent [48], hence, the high presence of its oxide further justifies the high ash content observed in the proximate analysis. Other notable oxides include MgO (6.57%) and Fe_2O_3 (4.65%). The presence of the oxides of N, P, and K suggests that BHB can be an excellent source of organic manure for soil amendment and to increase soil fertility [49]. Similar result was reported for rice husk by Hossain et al. [50].

3.2 Batch adsorption studies

3.2.1 pH and pH_{pzc} effect

Assessing both the pH range and pH_{pzc} is essential because each parameter describes a different but complementary aspect of the adsorption process. The pH study identifies the practical conditions under which the adsorbent exhibits its highest removal efficiency, while pHpzc provides insight into the surface charge behavior that controls electrostatic interactions between the biochar and ionic species.

The pH of the solution is a crucial factor in the adsorption process as it influences the solubility of metal ions, the concentration of counter ions on the adsorbent's functional groups, and the ionization degree of the adsorbent during the reaction [51]. Figure 5a illustrates how varying the pH of the solution influences the sorption of Pb(II) and Cr(VI) ions. For Pb(II), removal efficiency gradually rose from 54.2% to 94.7% as the pH surged from 2.0 to 8.0, with little to no further improvement observed between pH 8.0 and 9.0. In the case of Cr(VI), rate of elimination improved from 80.7% to 91.5% as the pH rose from 2.0 to 3.0, but beyond pH 3.0, the efficiency dropped sharply. These variation in optimum pH levels can be explained using the biochar's pH_{pzc}.

The point of zero charge (pH_{pzc}) refers to the pH at which the net surface charge of the adsorbent is neutral. Below this pH, the surface becomes positively charged due to protonation; above it, the surface develops a negative charge as a result of deprotonation

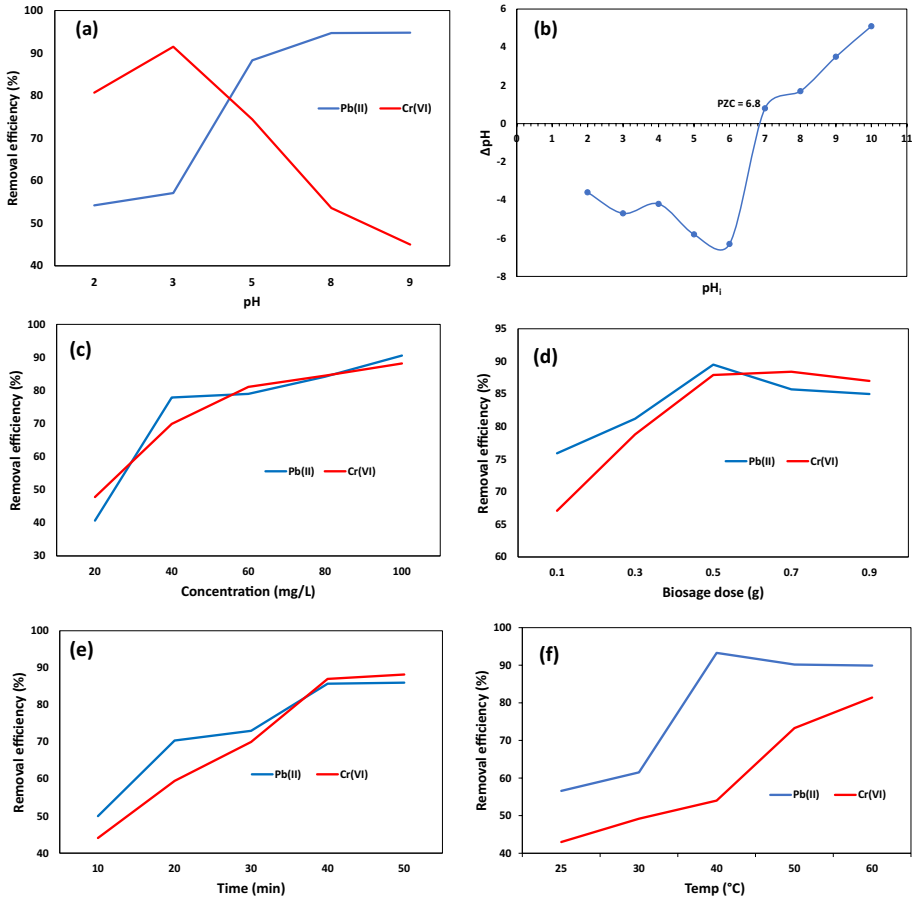


Fig. 5 Impact of process parameters on Pb(II) and Cr(VI) sorption **a** Solution pH **b** pH_{pzc} of BHB **c** starting metal ion concentrations **d** Biochar amount **e** Contact time **f** Temperature (Conditions: C_o= 100 mg/L, T = 25 ℃, t = 50 min, pH = 8.0 for Pb(II) and 3.0 for Cr(VI), biochar dose = 0.5 g)

[52]. The pH_{pzc} for BHB is 6.8 (Fig. 5b). This implies that at pH values greater than 6.8, the biochar surface is negatively charged, enhancing the adsorption of positively charged ions like Pb(II) through electrostatic attraction. This explains the observed higher adsorption efficiency for Pb(II) at pH values between 8 and 9, where the biochar surface carries a negative charge, and facilitates stronger electrostatic attraction with the positively charged Pb(II) ions [53]. On the contrary, for anions like Cr(VI), which exist as $HCrO_4^-$, CrO_4^{2-}, and $Cr_2O_7^{2-}$ depending on the solution pH, BHB would be more effective at pH values lower than 6.8. The acidic conditions protonate the biochar surface, creating positively charged adsorption sites that electrostatically attract chromate species. More OH- will be produced as the pH rises to an alkaline level (beyond the pH_{pzc}), which will repel the chromate ions and reduce the uptake effectiveness. This explains the cause of the sharp drop in Cr(VI) elimination rate when pH rose from 3.0 to 8.0. Consequently, the ideal pH for Pb(II) uptake was determined to be 8.0, and the ideal pH for Cr(VI) was determined to be 3.0. This behavior is consistent with previous studies showing that protonation of biochar surfaces under acidic conditions enhances the adsorption of chromate oxyanions through electrostatic interactions and subsequent surface complexation [12, 20, 54].

3.2.2 Effect of starting metal ion concentrations

The influence of the starting concentrations of metal ions is an important factor in adsorption processes, as it provides the concentration gradient necessary to drive Pb(II) and Cr(VI) ions toward the biochar surface [55]. Figure 5c illustrates how varying the initial concentrations affects adsorption. A sharp rise in Pb(II) uptake was noticed as the concentration increased from 20 to 40 mg/L. Beyond this point, the efficiency continued to improve more steadily until reaching a peak of 90.6% at 100 mg/L. In the case of Cr(VI), the removal also increases linearly with increasing initial concentration, reaching a peak removal efficiency of 88.2% at 100 mg/L. With higher initial concentrations, there are more metal ions available to interact with the biochar's available sorption sites, thus leading to a greater amount of metal ions being removed from the solution at higher concentrations. The observed trend may also be attributed to electrostatic attractions between the negatively charged metal ions and the adsorbent surface, which help to overcome diffusion resistance and promote mass transfer from the solution to the adsorbent [16].

3.2.3 Effect of biochar dosage

Biochar dosage is a critical factor in adsorption studies, as it directly affects the balance between the adsorbent and the contaminant in solution. Higher sorption effectiveness is often the consequence of increasing the adsorbent dosage, which also increases the quantities of surface functionalities and attachment sites on the adsorbent's surface [56]. The study's findings regarding the effect of adsorbent dosage on the sorption of Pb(II) and Cr(VI) ions using BHB are shown in Fig. 5d. As the amount of biochar elevated, so did the sorption effectiveness of both metal ions. Pb(II) highest uptake efficiency of 89.5% was recorded at a biochar dose of 0.5 g. This value reduced slightly to 85.7% and 85% at biochar doses of 0.7 and 0.9, respectively. For Cr(VI), the maximum efficiencies of 87.9% and 88.4% were respectively achieved at biochar doses of 0.5 and 0.7 g, which dropped marginally to 87% at 0.9 g. The higher number of accessible sorption sites at

higher doses is responsible for the improved efficiency; nevertheless, site saturation and particle aggregation cause the efficiency levels to slightly decline above 0.5 g for Pb(II) and 0.7 g for Cr(VI). The findings were comparable to those found in earlier research [57, 58].

3.2.4 Effect of contact time

Adsorption kinetics and equilibrium time are commonly determined by the impact of contact time on adsorption efficiency. Over time, the biochar's sorption efficiencies of both metal ions improved, as seen by the impact of contact time (Fig. 5e). For Pb(II) and Cr(VI), the efficiency rose substantially from 50 to 85.7% and 44.1 to 87%, respectively, as the contact time extended from 10 to 40 min. Beyond this point, there was no discernible improvement in the removal efficiencies; as the contact time rose to 50 min, Pb(II) efficiency almost remained constant at 86%, while Cr(VI) efficiency marginally increased to 88.2%. The fast initial uptake is likely a result of large number of readily accessible, which become saturated over time, leading to a slower rate of adsorption as equilibrium approaches [59]. These findings led to the selection of a 50-minute contact time for subsequent tests.

3.2.5 Effect of temperature

Among the crucial factors influencing the rate of adsorption is temperature. Raising a solution's temperature causes the viscosity to drop and the pollutant's diffusion rate to rise [60]. The temperature effect on Pb(II) and Cr(VI) sorption onto BHB was studied within the range of 25 to 60 ℃ (298–333 K), with the findings displayed in Fig. 5f. There was rapid removal of Pb(II) between 30 and 40 ℃, with a maximum removal efficiency of 93.3% observed at 40 ℃. This suggests an endothermic reaction. However, raising the temperature beyond 40 °C led to a decline in the efficiency of Pb(II) adsorption. For Cr(VI), the efficiency increased gradually throughout the temperature range, achieving a maximum removal efficiency of 81.4% at 60 ℃. The effective collision between the adsorbed metal ion and the biochar explains why Cr(VI) adsorption is more favorable at elevated temperatures [61].

3.3 Adsorption isotherm study

Adsorption isotherms illustrate the correlation between the amount of solute retained on the adsorbent surface and its concentration in solution at a constant temperature. In this study, three models, namely Langmuir, Freundlich, and Temkin, were employed to interpret the equilibrium data. The corresponding linear plots are depicted in Fig. 6, with the extracted parameters summarized in Table 2. Among the models, the Freundlich isotherm provided the best fit for the experimental data, indicating that adsorption occurred on a heterogeneous surface with sites possessing different adsorption energies. For Pb(II) adsorption, the correlation coefficients (R^2) were 0.9843 for Freundlich, 0.9707 for Langmuir, and 0.8992 for Temkin, while for Cr(VI), they are 0.9395, 0.9063, and 0.8797, respectively. The higher R^2 values for the Freundlich model suggested that adsorption took place on adsorbent surfaces with varying energy levels, involving multilayer adsorption through electrostatic interactions between previously adsorbed metal ions and those remaining in the solution [62]. The highest monolayer adsorption capacities recorded were 18.38 mg/g for Pb(II) and 22.78 mg/g for Cr(VI). To evaluate how

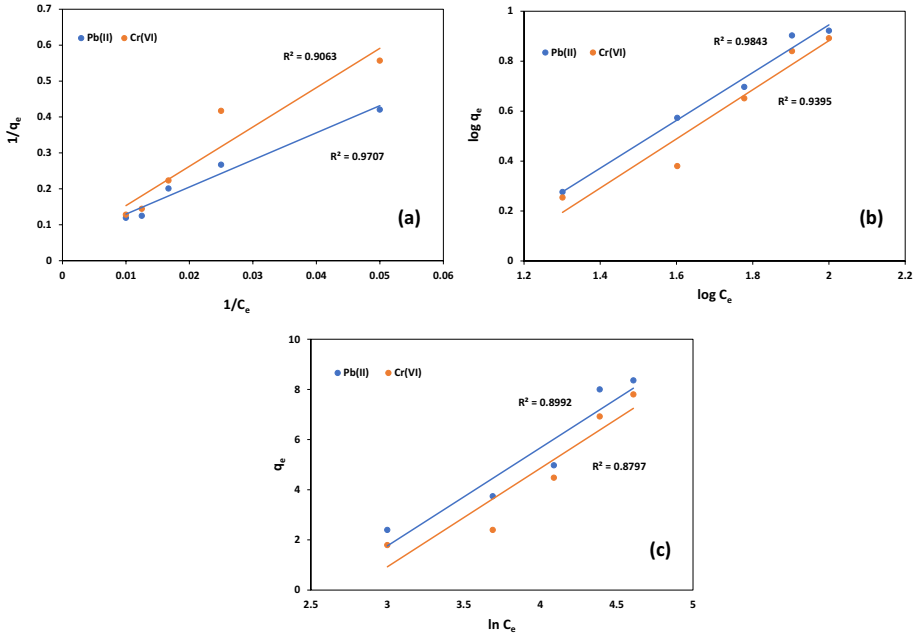


Fig. 6 **a** Langmuir, **b** Freundlich, and **c** Temkin graphs illustrating the sorption behavior of Pb(II) and Cr(VI) on BHB

Table 2 Isotherm characteristics governing the sorption of Pb(II) and Cr(VI) by BHB

Isotherm	Parameters	Pb(II)	Cr(VI)
Langmuir	q_{max} (mg/g)	18.38	22.78
	K_L (L/mg)	0.0072	0.00401
	R_L	0.581	0.714
	R^2	0.9707	0.9063
Freundlich	K_F (L/g)	0.380	0.5224
	n	1.046	1.182
	1/n	0.956	0.846
	R^2	0.9843	0.9395
Temkin	K_T (L/g)	0.0782	0.0631
	B (J/mol)	3.903	3.923
	b_T (J/mol)	634.79	631.61
	R^2	0.8992	0.8797

favorable the adsorption was, the separation factor (R_L) was calculated. According to standard interpretation, an R_L value of 1 indicates a linear process, 0 suggests irreversibility, values greater than 1 imply an unfavorable process, and values between 0 and 1 signify favorable adsorption [55]. In this study, R_L values for both metal ions fell within the $0 < R_L < 1$ range, signifying the favorable nature of the adsorption. This conclusion is further supported by the Freundlich constant (n), which was greater than 1 for both metal ions, indicating strong adsorption intensity. An adsorbent is considered favorable for pollutant uptake if n ranges between 1 and 10 [63].

For the Temkin model, the values of the constant related to the heat of adsorption B are 3.903 and 3.923 J/mol for Pb(II) and Cr(VI), respectively. These values are relatively low, suggesting that the adsorption was predominantly physical, with moderate interactions between the biochar surface and metal ions. This aligns with earlier reports where low B values indicated physisorption-driven processes dominated by ion exchange and electrostatic attraction rather than chemical bonding [64, 65]. However, the Temkin

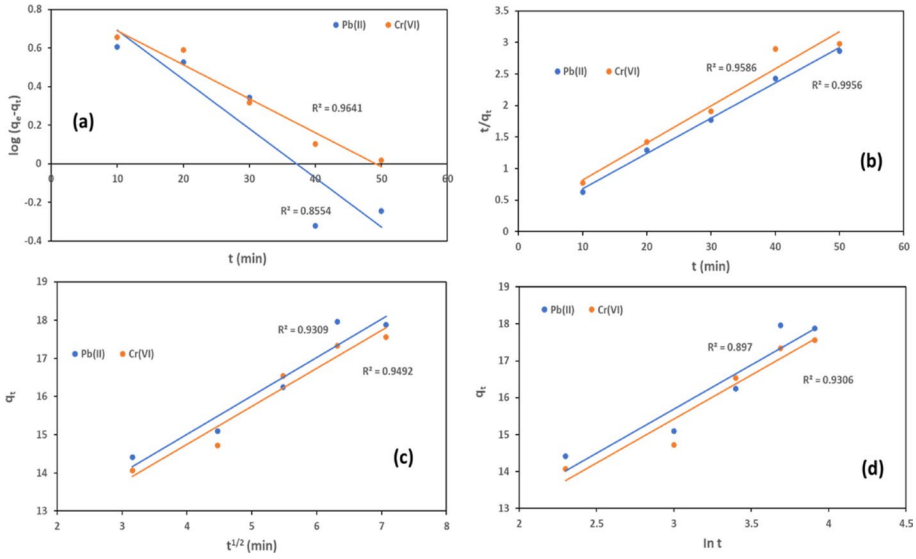


Fig. 7 **a** PFO **b** PSO **c** IPD and **d** Elovich models for the sorption of Pb(II) and Cr(VI) onto BHB

Table 3 Kinetic characteristics governing the sorption of Pb(II) and Cr(VI) by BHB

Kinetics	Parameters	Pb(II)	Cr(VI)
Pseudo-first-order	K_1	0.0255	0.0177
	q_e (exp.) (mg/g)	16.38	11.44
	q_e (cal.) (mg/g)	18.45	15.60
	R^2	0.8554	0.9641
Pseudo-second-order	K_2	0.0271	0.0152
	q_e (exp.) (mg/g)	16.38	11.44
	q_e (cal.) (mg/g)	17.83	16.98
	R^2	0.9956	0.9586
Intraparticle diffusion	K_{dif}	1.0054	0.9961
	C	10.99	10.76
	R^2	0.9309	0.9492
Elovich	β	0.418	0.419
	α	84.56	75.93
	R^2	0.8970	0.9306

model gave the lowest R^2 values among the three isotherms, suggesting that although surface interactions influenced adsorption, the energetic heterogeneity of the biochar adsorbent was more accurately captured by the Freundlich isotherm.

3.4 Adsorption kinetic study

Kinetic modeling helps to understand how quickly an adsorbent interacts with and removes target contaminants over time. In this study, the adsorption behavior of Pb(II) and Cr(VI) on bean husk biochar (BHB) was evaluated using four kinetic models: PFO, PSO, IPD, and Elovich equation. Graphical representations of these models are shown in Fig. 7, while their calculated parameters are provided in Table 3. The derived kinetic constants and fit quality were used to interpret the dominant adsorption mechanism and identify the rate-limiting step in the process. For Pb(II), the PSO model provides the better fitting with R^2 value of 0.9956, which is higher than that of IPD (0.9309), Elovich (0.8970), and PFO models (0.8554), in that order. This higher degree of fit with the PSO

model indicates that the adsorption of Pb(II) likely proceeds via chemisorption, involving electron sharing or exchange between the biochar and the metal ions [66]. Also, the calculated q_e value for the PSO (17.83 mg/g) closely matches the experimentally observed value (16.38 mg/g) than that of the PFO (18.45 and 16.38 mg/g for calculated and experimental, respectively), which further supports the PSO model as the more suitable fit than the PFO model for Pb(II) adsorption.

For Cr(VI), the PFO model provides a better fit for BH (R^2 = 0.9641) than the PSO (R^2 = 0.9586), suggesting that the adsorption of Cr(VI) onto BHB occurs majorly via weaker physical interactions such as van der Waals forces. Again, the calculated q_e value from the PFO model (15.60 mg/g) more closely aligns with the actual experimentally observed value (11.44 mg/g), confirming its suitability over the PSO model for describing Cr(VI) uptake by BHB. To further investigate the mechanism, the IPD model was applied to determine the rate-limiting step. A truly diffusion-controlled process would show a linear plot passing through the origin [67]. Herein, it is evident that the plot diverged from the origin, indicating that rate-controlling steps were not limited to intraparticle diffusion. Similar findings were reported by Neeli et al. [68], where the sorption of Pb(II), Cr(VI), and As(V) by cellulose-based biochar followed PSO kinetics, whereas Cu(II) was best described by the PFO model.

3.5 Adsorption thermodynamic study

Thermodynamic analysis was performed by altering the temperature and evaluating key indicators such as Gibbs free energy (ΔG), enthalpy (ΔH), and entropy (ΔS). These variables help determine the spontaneity, energetic nature, and underlying mechanism of the adsorbate–adsorbent interaction [69]. From the Van't Hoff plot of *ln* Kc versus 1/T (Figure S1), the slope and intercept were respectively used to derive ΔH and ΔS. The corresponding thermodynamic values are summarized in Table 4. The consistently negative ΔG values for both BH and BHP across the tested temperatures confirm that the adsorption is thermodynamically favorable and occurs spontaneously. These values become more negative as the temperature increases from 298 K to 333 K, ranging from − 60.47 to −68.93 kJ/mol for Pb(II) and from − 32.66 to -37.05 kJ/mol for Cr(VI). This implies that the adsorption becomes progressively more thermodynamically favorable at elevated temperatures [70]. The positive ΔH values confirm that the adsorption is an endothermic process. Likewise, the positive ΔS values indicate increased molecular disorder at the interface between the biochar surface and the aqueous phase during the adsorption process [71].

Table 4 Thermodynamic-dependent factors for Pb(II) and Cr(VI) sorption onto BHB

Sample	Temperature (K)	ΔG (kJ/mol)	ΔH (kJ/mol)	ΔS (J/mol.K)
Pb(II)	298	−60.47	65.61	203.1
	303	−61.49		
	313	−64.53		
	323	−66.56		
	333	−68.93		
Cr(VI)	298	−32.66	37.61	109.7
	303	−33.21		
	313	−34.86		
	323	−35.96		
	333	−37.05		

3.6 Regeneration and reuse of BHB

Adsorbent regeneration is the process by which an adsorbent can be restored and used several times without losing its effectiveness. This step is essential in water purification systems because it guarantees the sustainability of the adsorbent and its cost-effectiveness throughout several cycles of pollutant removal. The results of three successive adsorption-desorption cycles of the biochar adsorbent are shown in Figure S2. In the first cycle, HNO_3 desorbs 87.9% of Pb(II) and 89.4% of Cr(VI). The following cycles saw a decline in these levels. This relatively high desorption observed in acidic medium can be explained by the prevalence of negatively charged sites on the biochar surface, along with metal ions loosely attached to mildly positive functional groups. These metal ions are readily displaced by the more competitive hydrogen ions (H^+) present in the acidic environment [72]. A similar pattern was observed in the adsorption cycle, where BHB removed 88.5% of Pb(II) and 91% of Cr(VI) in the first cycle, maintaining 63% and 70.1% removal even after the third round. The initial cycle exhibits high adsorption efficiency due to the abundance of available pores and binding sites on the adsorbent's surface. However, as the adsorption process continues through subsequent cycles, these sites become increasingly occupied, leading to a gradual decline in removal efficiency.

3.7 Possible mechanism of adsorption

The mechanisms underlying the sorption of Pb(II) and Cr(VI) onto the surfaces of BHB were examined using several methods, including isotherm and kinetic models, thermodynamic studies, pH_{pzc}, and spectroscopic analyses, among others. Initially, FTIR research showed that the biochar has a number of oxygenated functional groups, including -OH, C = O, and -COOH, which can help metal ions in solution adsorb. Comparison of FTIR spectra before and after adsorption reveals clear involvement of these oxygen-containing surface functionalities in metal uptake. The O-H band shifted from 3435 to 3305 cm^{-1}, carbonyl and aromatic bands near 1738 and 1601 cm^{-1} were displaced, and the C-O region (1216–1384 cm^{-1}) showed notable changes. These groups have the ability to liberate H^+ from the biochar surface, which will allow for the binding of Pb(II) ions. The appearance of new low-frequency bands around 593 and 529 cm^{-1} further indicates the formation of metal-oxygen linkages, providing evidence for the formation of surface-bound Pb-O and Cr-O species. As observed in the pH_{pzc} analysis, the biochar surface becomes protonated at pH levels above pH_{pzc} of BHB, leading to enhanced Pb(II) adsorption. These findings indicate that ion exchange was a dominant mechanism in the removal of Pb(II), with additional contribution from complex formation between Pb(II) ions and oxygen-based functionalities on the biochar surface. Thermodynamic analysis revealed the process to be both spontaneous and endothermic, pointing to the stable binding of Pb(II) via surface complexation.

In contrast, Cr(VI), which exists in aqueous systems as anions (CrO_4^{2-} or $Cr_2O_7^{2-}$), is likely removed through its reduction to the less harmful Cr(III). Under acidic conditions (below pH_{pzc}), the biochar's surface becomes positively charged due to protonation of functional groups like $-OH_2^+$ and $-COOH_2^+$, allowing Cr(VI) to be adsorbed electrostatically. After initial adsorption, Cr(VI) species are reduced to Cr(III), which subsequently interacts with the surface functionalities to form stable complexes [61]. This is confirmed by the emergence of metal-oxygen bands in the FTIR spectrum. Additionally, the alignment of Cr(VI) adsorption data with the PFO kinetic model suggests that weak

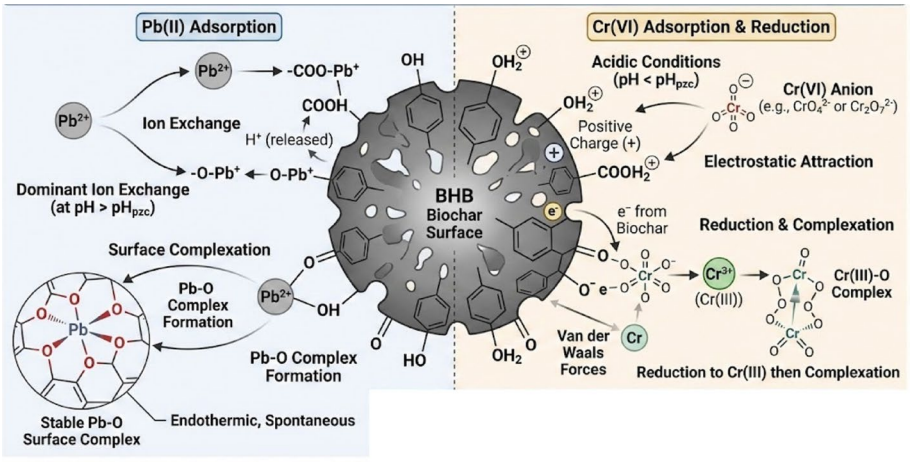


Fig. 8 Schematic representation of the proposed adsorption mechanism for Pb(II) and Cr(VI) by BHB

Table 5 Maximum adsorption capacites of Pb(II) and Cr(VI) onto various sorbents

Adsorbent	q_{max} (mg/g)		References
	Pb(II)	Cr(VI)	
Apricot kernel	23.9	12.7	[73]
Plum kernel	28.8	14.0	[73]
Palm oil sludge biochar	20.87	–	[74]
Iron oxide/typha biochar	–	32.82	[61]
Fe nanoparticles/cellulose biochar	17.3	18.5	[68]
Wheat straw biochar	–	24.60	[75]
Wheat straw biochar + Fe_3O_4	73.34	–	[10]
Bean husk biochar	18.38	22.78	This study

intermolecular attractions, such as van der Waals forces, also contributed to the process. Therefore, we propose that the retention of Pb(II) and Cr(VI) on BHB likely results from multiple simultaneous processes, such as ion exchange, electrostatic interactions, surface complexation, and non-specific physical adsorption, among others. The proposed mechanism is schematically shown in Fig. 8.

3.8 Comparison with other adsorbents

Table 5 compares different biomass-derived biochars' adsorptive capacities for Pb(II) and Cr(VI) adsorption. As can be seen, the uptake capacities of various adsorbents differ considerably, and in comparison, the BHB shows a good ability in eliminating Pb(II) and Cr(VI) ions. However, while BHB exhibits a reasonable surface area, its adsorption capacity for Pb(II) and Cr(VI) is lower than that of some reported biochar adsorbents reported in the literature, particularly chemically modified biochars. This difference arises because adsorption is influenced not only by surface area but also by surface chemistry and pore structure. Modified biochars often possess additional functional groups or enhanced microporosity, which provide more active sites and stronger interactions with metal ions. Nevertheless, modified adsorbents often result in higher operation costs. Thus, this presents BHB as a viable and economical alternative for extracting Pb(II) and Cr(VI) from water, particularly in situations where the adsorbent's cost and environmental impact are important factors to consider.

4 Conclusion

This research explored the synthesis and evaluation of biochar produced from bean husk residues for its potential in eliminating Pb(II) and Cr(VI) ions from water. The biochar exhibited a surface area of 24.28 m^2/g and remove Pb(II) at pH 8 with 94.7% efficiency and Cr(VI) at pH 3 with 91.5% efficiency when 50 min, 0.5 g of biochar, and 25 °C were the optimal conditions. The maximum monolayer uptake capacities reached 18.38 mg/g for Pb(II) and 22.78 mg/g for Cr(VI), with the adsorption behavior following the Freundlich isotherm model for both metal ions. The kinetic analysis indicated that Pb(II) adsorption followed the pseudo-second order model, while Cr(VI) adsorption aligned with the pseudo-first order model. The adsorbent demonstrated promising reusability, maintaining up to 60% efficiency after three cycles. Pb(II) adsorption was primarily driven by ion exchange and the formation of surface-bound complexes, whereas Cr(VI) removal was influenced by electrostatic interactions, physical adsorption, reduction of Cr(VI) to Cr(III), and subsequent complexation.

Supplementary Information

The online version contains supplementary material available at https://doi.org/10.1007/s44371-026-00930-z.

Supplementary Material 1.

Acknowledgements

The authors acknowledge the grant owners who partly supported this research. Firstly, the Competitive Programme for Rated Researchers (CPRR) Grant, Reference Number: SRUG2204092895, owned by Prof. Z. Caliphs, was utilized for sample analysis. Secondly, the Research and Publication Grant, Number 086225, owned by Prof. Jane Catherine Ngila, funded travel expenses during Prof. H.K. Okoro's research visit to the University of Johannesburg.

Author contributions

H.K.O. and A.G.A. conceptualized and supervised the study. E.C.E. performed the experiment and wrote the main text. K.O.I. and J.E. interpreted the data. C.Z. and C.J.N. carried out analytical techniques and funded the study. All authors reviewed the manuscript.

Funding

This work received no external funding.

Data availability

All data generated or analysed during this study are included in this published article [and its supplementary information files].

Declarations

Ethics approval and consent to participate

Not applicable.

Consent for publication

Not applicable.

Competing interests

The authors declare no competing interests.

Received: 24 September 2025 / Accepted: 18 August 2026



References

1. Sankhla MS, Kumari M, Nandan M, Kumar R, Agrawal P. Heavy metals contamination in water and their hazardous effect on human health-a review. Int J Curr Microbiol App Sci. 2016;5(10):759–66.
2. Emenike EC, Iwuozor KO, Anidiobi SU. Heavy metal pollution in aquaculture: sources, impacts and mitigation techniques. Biol Trace Elem Res, 2021;1–17.
3. Sharma A, Grewal AS, Sharma D, Srivastav AL. In: Water M, Shukla SK, et al. editors. Chap. 3 - Heavy metal contamination in water: consequences on human health and environment. Elsevier; 2023;39–52. https://doi.org/10.1016/B978-0-323-95919-3.00015-X.

4. Debnath B, Singh WS, Manna K. Sources and toxicological effects of lead on human health. Indian J Med Specialities. 2019;10(2):66–71.
5. Sreekala G, Beevi AF, Resmi R, Beena B. Removal of lead (II) ions from water using copper ferrite nanoparticles synthesized by green method. Mater Today: Proc. 2021;45:3986–90.
6. Rai PK. Heavy metal phytoremediation from aquatic ecosystems with special reference to macrophytes. Crit Rev Environ Sci Technol. 2009;39(9):697–753.
7. Srivastava S, Agrawal SB, Mondal MK. Characterization, isotherm and kinetic study of Phaseolus vulgaris husk as an innovative adsorbent for Cr (VI) removal. Korean J Chem Eng. 2016;33:567–75.
8. Ma L, Chen N, Feng C, Yang Q. Recent advances in enhanced technology of Cr (VI) bioreduction in aqueous condition: A review. Chemosphere. 2024;351:141176.
9. Xie S. Water contamination due to hexavalent chromium and its health impacts: exploring green technology for Cr (VI) remediation. Green Chem Lett Rev. 2024;17(1):2356614.
10. Li Y, Zhang X, Zhang P, Liu X, Han L. Facile fabrication of magnetic bio-derived chars by co-mixing with Fe3O4 nanoparticles for effective Pb2 + adsorption: properties and mechanism. J Clean Prod. 2020;262:121350.
11. Zhang X, Wu S, Liu Y, Wang Z, Zhang H, Xiao R. Removal of Cr (VI) from aqueous solution by Rice-husk-based activated carbon prepared by Dual-mode heating method. Carbon Resour Convers. 2023;6(2):76–84.
12. Pochampally SV, Letourneau E, Abdulraheem I, Monk J, Sims D, Murph SEH, Marti EJ, Moon J. Metal-organic-framework and walnut shell biochar composites for lead and hexavalent chromium removal from aqueous environments. Chemosphere. 2024;367:143572.
13. Iwuozor KO, Ighalo JO, Emenike EC, Ogunfowora LA, Igwegbe CA. Adsorption of methyl orange: A review on adsorbent performance. Curr Res green sustainable Chem. 2021;4:100179.
14. Soudani A, Youcef L, Bulgariu L, Youcef S, Toumi K, Soudani N. Characterizing and modeling of oak fruit shells biochar as an adsorbent for the removal of Cu, Cd, and Zn in single and in competitive systems. Chem Eng Res Des. 2022;188:972–87. https://doi.org/10.1016/j.cherd.2022.10.009.
15. Bonilla-Petriciolet A, Mendoza-Castillo DI. and H.E. Reynel-Ávila, Adsorption processes for water treatment and purification. Springer; 2017;256.
16. Emenike EC, Adeniyi AG, Iwuozor KO, Okorie CJ, Egbemhenghe AU, Omuku PE, Okwu KC, Saliu OD. A critical review on the removal of mercury (Hg2+) from aqueous solution using nanoadsorbents. Environmental Nanotechnology, Monitoring & Management; 2023;100816.
17. Ghasemi SS, Hadavifar M, Maleki B, Mohammadnia E. Adsorption of mercury ions from synthetic aqueous solution using polydopamine decorated SWCNTs. J Water Process Eng. 2019;32:100965. https://doi.org/10.1016/j.jwpe.2019.100965.
18. Wang J, Wang S. Preparation, modification and environmental application of biochar: A review. J Clean Prod. 2019;227:1002–22.
19. Emenike EC, Okoro HK, Iwuozor KO, Egbemhenghe AU, Okwu KC, Adeniyi AG, Paul S, Akshaya K, Selvasembian R. Biowaste-derived biochars for treatment of wastewater contaminated by dyes, in Biochar for Environmental Remediation. Elsevier; 2025;191–213.
20. Agrafioti E, Kalderis D, Diamadopoulos E. Arsenic and chromium removal from water using biochars derived from rice husk, organic solid wastes and sewage sludge. J Environ Manage. 2014;133:309–14.
21. Jia Y, Shi S, Liu J, Su S, Liang Q, Zeng X, Li T. Study of the effect of pyrolysis temperature on the Cd2 + adsorption characteristics of biochar. Appl Sci. 2018;8(7):1019.
22. Oliveira FR, Patel AK, Jaisi DP, Adhikari S, Lu H, Khanal SK. Environmental application of biochar: Current status and perspectives. Bioresour Technol. 2017;246:110–22.
23. Adeniyi AG, Iwuozor KO, Emenike EC, Ajala OJ, Ogunniyi S, Muritala KB. Thermochemical co-conversion of biomass-plastic waste to biochar: a review. Green Chem Eng. 2024;5(1):31–49.
24. Mosoarca G, Popa S, Vancea C, Boran S. Optimization, equilibrium and kinetic modeling of methylene blue removal from aqueous solutions using dry bean pods husks powder. Materials. 2021;14(19):5673.
25. Elaigwu S, Shokunbi O. Composting of dry bean (Phaseolus vulgaris) husk: Physicochemical and spectroscopic characterisation. 2017.
26. Bello OS, Alao OC, Alagbada TC, Olatunde AM. Biosorption of ibuprofen using functionalized bean husks. Sustainable Chem Pharm. 2019;13:100151.
27. Singh V, Pant N, Sharma RK, Padalia D, Rawat PS, Goswami R, Singh P, Kumar A, Bhandari P, Tabish A. Adsorption studies of Pb (II) and Cd (II) heavy metal ions from aqueous solutions using a magnetic biochar composite material. Separations. 2023;10(7):389.
28. Tho P, Van HT, Nguyen LH, Hoang TK, Tran TNH, Nguyen TT, Nguyen TBH, Nguyen VQ, Le Sy H, Thai VN. Enhanced simultaneous adsorption of As (iii), Cd (ii), Pb (ii) and Cr (vi) ions from aqueous solution using cassava root husk-derived biochar loaded with ZnO nanoparticles. RSC Adv. 2021;11(31):18881–97.
29. Venkatraman Y, Arunkumar P, Kumar NS, Osman AI, Muthiah M, Al-Fatesh AS, Koduru JR. Exploring modified rice straw biochar as a sustainable solution for simultaneous Cr (VI) and Pb (II) removal from wastewater: Characterization, mechanism insights, and application feasibility. ACS omega. 2023;8(41):38130–47.
30. Emenike EC, Okoro HK, Adeniyi AG, Iwuozor KO, Zvinowanda C, Ngila JC. Applications of bean pod and husk for remediation of water contamination: a review. Bioresource Technol Rep. 2024;25:101754.
31. Emenike EC, Iwuozor KO, Agbana SA, Otoikhian KS, Adeniyi AG. Efficient recycling of disposable face masks via co-carbonization with waste biomass: a pathway to a cleaner environment. Clean Environ Syst. 2022;6:100094.
32. Jian X, Zhuang X, Li B, Xu X, Wei Z, Song Y, Jiang E. Comparison of characterization and adsorption of biochars produced from hydrothermal carbonization and pyrolysis. Volume 10. Environmental Technology & Innovation; 2018;27–35.
33. Bahrami M, Amiri MJ, Beigzadeh B. Adsorption of 2, 4-dichlorophenoxyacetic acid using rice husk biochar, granular activated carbon, and multi-walled carbon nanotubes in a fixed bed column system. Water Sci Technol. 2018;78(8):1812–21.
34. Langmuir I. The adsorption of gases on plane surfaces of glass, mica and platinum. J Am Chem Soc. 1918;40(9):1361–403.
35. Temkin M, Pyzhev V. Recent modifications to Langmuir isotherms. 1940.
36. Ho Y-S, McKay G. Pseudo-second order model for sorption processes. Process Biochem. 1999;34(5):451–65.
37. Ajmal Z, Muhmood A, Dong R, Wu S. Probing the efficiency of magnetically modified biomass-derived biochar for effective phosphate removal. J Environ Manage. 2020;253:109730.

38. Amoloye MA, Abdulkareem SA, Adeniyi AG. A Study on the Kinetics and Effects of Three Combustion Fuels on Retort Carbonization of Corn Husk and Cob. J Renew Energy Environ. 2024;11(2):89–101.
39. Adeniyi AG, Abdulkareem SA, Ighalo JO, Onifade DV, Sanusi SK. Thermochemical Co-conversion of Sugarcane Bagasse-LDPE Hybrid Waste into Biochar. Arab J Sci Eng. 2021;46(7):6391–7. https://doi.org/10.1007/s13369-020-05119-9.
40. Adeniyi AG, Emenike EC, Agbana SA, Iwuozor KO, Saliu OD. Evaluation of the properties of solid biofuel produced from coconut fibre. Indian Chem Eng, 2023;1–12.
41. Ighalo JO, Conradie J, Ohoro CR, Amaku JF, Oyedotun KO, Maxakato NW, Akpomie KG, Okeke ES, Olisah C, Malloum A. Biochar from coconut residues: An overview of production, properties, and applications. Ind Crops Prod. 2023;204:117300.
42. Kizito S, Wu S, Kirui WK, Lei M, Lu Q, Bah H, Dong R. Evaluation of slow pyrolyzed wood and rice husks biochar for adsorption of ammonium nitrogen from piggery manure anaerobic digestate slurry. Sci Total Environ. 2015;505:102–12.
43. Xiang J, Lin Q, Cheng S, Guo J, Yao X, Liu Q, Yin G, Liu D. Enhanced adsorption of Cd (II) from aqueous solution by a magnesium oxide–rice husk biochar composite. Environ Sci Pollut Res. 2018;25:14032–42.
44. Banu HT, Karthikeyan P, Meenakshi S. Zr4 + ions embedded chitosan-soya bean husk activated bio-char composite beads for the recovery of nitrate and phosphate ions from aqueous solution. Int J Biol Macromol. 2019;130:573–83.
45. Huong PT, Jitae K, Al Tahtamouni T, Tri NLM, Kim H-H, Cho KH, Lee C. Novel activation of peroxymonosulfate by biochar derived from rice husk toward oxidation of organic contaminants in wastewater. J Water Process Eng. 2020;33:101037.
46. Sooksawat N, Santibenchakul S, Kruatrachue M, Inthorn D. Recycling rice husk for removal of phosphate and nitrate from synthetic and swine wastewater: Adsorption study and nutrient analysis of modified rice husk. J Environ Sci Health Part A. 2021;56(10):1080–92.
47. Babu K, Nataraj M, Tayappa Y, Vyas RK, Mishra, Acharya B. Production of biochar from waste biomass using slow pyrolysis: Studies of the effect of pyrolysis temperature and holding time on biochar yield and properties. Mater Sci Energy Technol. 2024;7:318–34.
48. Rahmat A, Hidayat H, Kurniawan K, Hariadi H, Nuraini L, Rahmadya A, Prasetia H, Nurtanto M, Suhendar U. X-ray fluorescence analysis of coconut wood sawdust and coconut coir dust biochar prepared under low-temperature pyrolysis. in AIP Conference Proceedings. 2024. AIP Publishing.
49. Tran H-T, Bolan NS, Lin C, Binh QA, Nguyen M-K, Luu TA, Le V-G, Pham CQ, Hoang H-G, Vo D-VN. Succession of biochar addition for soil amendment and contaminants remediation during co-composting: A state of art review. J Environ Manage. 2023;342:118191.
50. Hossain N, Nizamuddin S, Griffin G, Selvakannan P, Mubarak NM, Mahlia TMI. Synthesis and characterization of rice husk biochar via hydrothermal carbonization for wastewater treatment and biofuel production. Sci Rep. 2020;10(1):18851.
51. Meng Y, Chen D, Sun Y, Jiao D, Zeng D, Liu Z. Adsorption of Cu2 + ions using chitosan-modified magnetic Mn ferrite nanoparticles synthesized by microwave-assisted hydrothermal method. Appl Surf Sci. 2015;324:745–50.
52. Emenike EC, Adeniyi AG, Omuku PE, Okwu KC, Iwuozor KO. Recent advances in nano-adsorbents for the sequestration of copper from water. J Water Process Eng. 2022;47:102715.
53. Phuong D, Loc N, Miyanishi T. Efficiency of dye adsorption by biochars produced from residues of two rice varieties, Japanese Koshihikari and Vietnamese IR50404. Desalination Water Treat. 2019;165:333–51.
54. Emenike EC, Okoro HK, Al-Senani GM, Al-Qahtani SD, Iwuozor KO, Egbemhenghe AU, Emeghai J, Adeniyi AG. Adsorptive removal of Cr (VI) and Pb (II) using biochar from biomass and plastic waste: characterization and performance evaluation. Biomass Bioenergy. 2026;207:108722.
55. Khalil U, Shakoor MB, Ali S, Rizwan M, Alyemeni MN, Wijaya L. Adsorption-reduction performance of tea waste and rice husk biochars for Cr (VI) elimination from wastewater. J Saudi Chem Soc. 2020;24(11):799–810.
56. Razavi Z, Mirghaffari N, Rezaei B. Adsorption of crude and engine oils from water using raw rice husk. Water Sci Technol. 2014;69(5):947–52.
57. Zhang L, Ren Y, Xue Y, Cui Z, Wei Q, Han C, He J. Preparation of biochar by mango peel and its adsorption characteristics of Cd (II) in solution. RSC Adv. 2020;10(59):35878–88.
58. Hevira L, Ighalo JO, Sondari D. Adsorption indigo carmine using chitosan from black soldier fly (Hermetia illucens L.): Insights into scalable application in real wastewater systems. Inorg Chem Commun, 2025;114011.
59. Ogunniyi S, Emenike EC, Iwuozor KO, Ighalo JO, Ezzat AO, Adewoye TL, Egbemhenghe A, Okoro HK, Adeniyi AG. Removal of phenol from wastewater using Luffa cylindrica fibers in a packed bed column: Optimization, isotherm and kinetic studies. Heliyon, 2024;10(4).
60. Nassar NN. Iron oxide nanoadsorbents for removal of various pollutants from wastewater: an overview. Application of adsorbents for water pollution control, 2012;81–118.
61. Cai Y, Ran Z, Cang Y, Chen X, Shaaban M, Peng Q-A. Efficient removal of Cr (VI) and As (V) from an aquatic system using iron oxide supported typha biochar. Environ Res. 2023;225:115588.
62. Shooto ND, Nkutha CS, Guilande NR, Naidoo EB. Pristine and modified mucuna beans adsorptive studies of toxic lead ions and methylene blue dye from aqueous solution. S Afr J Chem Eng. 2020;31:33–43.
63. Onwordi CT, Uche CC, Ameh AE, Petrik LF. Comparative study of the adsorption capacity of lead (II) ions onto bean husk and fish scale from aqueous solution. J water reuse Desalin. 2019;9(3):249–62.
64. Liang X, Su Y, Wang X, Liang C, Tang C, Wei J, Liu K, Ma J, Yu F, Li Y. Insights into the heavy metal adsorption and immobilization mechanisms of CaFe-layered double hydroxide corn straw biochar: Synthesis and application in a combined heavy metal-contaminated environment. Chemosphere. 2023;313:137467.
65. Umeh CT, Nduka JK, Iwuozor OK, Omokpariola OD, Dulta K, Ezeh SC, Emeka RN. Adsorption modelling on the removal of ciprofloxacin antibiotic from aqueous solution by acid-modified corn cob. Int J Environ Anal Chem, 2023;1–26.
66. Ogunlalu O, Oyekunle IP, Iwuozor KO, Aderibigbe AD, Emenike EC. Trends in the mitigation of heavy metal ions from aqueous solutions using unmodified and chemically-modified agricultural waste adsorbents. Curr Res Green Sustainable Chem. 2021;4:100188.
67. Sadeghi Afjeh M, Bagheri Marandi G, Zohuriaan-Mehr MJ. Nitrate removal from aqueous solutions by adsorption onto hydrogel-rice husk biochar composite. Water Environ Res. 2020;92(6):934–47.
68. Neeli ST, Ramsurn H, Ng CY, Wang Y, Lu J. Removal of Cr (VI), As (V), Cu (II), and Pb (II) using cellulose biochar supported iron nanoparticles: A kinetic and mechanistic study. J Environ Chem Eng. 2020;8(5):103886.
69. Iwuozor K, Emenike E, Gbadamosi F, Ighalo J, Umenweke G, Iwuchukwu F, Nwakire C, Igwegbe C. Adsorption of organophosphate pesticides from aqueous solution: a review of recent advances. Int J Environ Sci Technol. 2023;20(5):5845–94.

70. Yadav BS, Dasgupta S. Effect of time, pH, and temperature on kinetics for adsorption of methyl orange dye into the modified nitrate intercalated MgAl LDH adsorbent. Inorg Chem Commun. 2022;137:109203.
71. Shooto ND, Thabede PM, Bhila B, Moloto H, Naidoo EB. Lead ions and methylene blue dye removal from aqueous solution by mucuna beans (velvet beans) adsorbents. J Environ Chem Eng. 2020;8(2):103557.
72. Zhang J, Wang Q. Sustainable mechanisms of biochar derived from brewers' spent grain and sewage sludge for ammonia–nitrogen capture. J Clean Prod. 2016;112:3927–34.
73. Pap S, Bezanovic V, Radonic J, Babic A, Saric S, Adamovic D, Sekulic MT. Synthesis of highly-efficient functionalized biochars from fruit industry waste biomass for the removal of chromium and lead. J Mol Liq. 2018;268:315–25.
74. Lee XJ, Lee LY, Hiew BYZ, Gan S, Thangalazhy-Gopakumar S, Ng HK. Multistage optimizations of slow pyrolysis synthesis of biochar from palm oil sludge for adsorption of lead. Bioresour Technol. 2017;245:944–53.
75. Tytłak A, Oleszczuk P, Dobrowolski R. Sorption and desorption of Cr (VI) ions from water by biochars in different environmental conditions. Environ Sci Pollut Res. 2015;22:5985–94.

Publisher's Note

Springer Nature remains neutral with regard to jurisdictional claims in published maps and institutional affiliations.